ISSN 0021-3640, JETP Letters, 2023, Vol. 118, No. 8, pp. 574–578. © Pleiades Publishing, Ltd., 2023.
ISSN 0021-3640, JETP Letters, 2023. © Pleiades Publishing, Ltd., 2023.
Russian Text © The Author(s), 2023, published in Pis'ma v Zhurnal Eksperimental'noi i Teoreticheskoi Fiziki, 2023, Vol. 118, No. 8, pp. 584–589.

CONDENSED MATTER

Spatially Inhomogeneous Ultrafast Demagnetization of a Nickel Magnetoplasmonic Crystal

I. A. Novikov[a] (ORCID: 0000-0002-7652-7816), M. A. Kiryanov[a] (ORCID: 0000-0002-4534-3491), A. Yu. Frolov[a] (ORCID: 0000-0003-0988-1361), V. V. Popov[a], T. V. Dolgova[a] (ORCID: 0000-0001-8981-0808), and A. A. Fedyanin[a,*] (ORCID: 0000-0003-4708-6895)

[a] *Faculty of Physics, Moscow State University, Moscow, 119991 Russia*

**e-mail: fedyanin@nanolab.phys.msu.ru*

Received August 17, 2023; revised September 8, 2023; accepted September 11, 2023

A 50% decrease in the magneto-optical Kerr effect is observed in the experiment on subpicosecond laser-induced demagnetization of the one-dimensional all-nickel magnetoplasmonic crystal. The femtosecond pulse energy density is comparable to that required to achieve similar values in thin films. Numerical calculations show that such a decrease is not governed by the uniform reduction of surface magnetization, but is the result of the appearance of demagnetized and non-demagnetized areas of the surface.

DOI: 10.1134/S0021364023602853

Experimental studies of ultrafast laser demagnetization have been started with the pioneer work on the observation of transient magneto-optical Kerr effect in a thin nickel film irradiated by femtosecond laser pulse [1]. The observed demagnetization time turned out to be significantly smaller than the period of magnetic moments precession. In almost three decades various concepts were introduced to describe the phenomenon, such as three-temperature model and various extensions of two-temperature model [1–3], Elliot–Yaffet spin-flip scattering [4–6], Landau–Lifshitz–Bloch equation [7], and time-dependent density functional theory [8–10]. The models predict similar demagnetization time values but conflict in estimations of required pulse energy density. Moreover, experimental [11, 12] and theoretical [13, 14] studies have shown the demagnetization state of metal films to be strongly dependent on their thickness.

Nanoscale systems support the excitation of various electromagnetic modes, which allows electromagnetic field concentration. Mie resonances [15, 16], bound states in continuum [17, 18], waveguide modes [19], Bloch surface waves [20], Tamm [21], localized [22, 23] and lattice [24, 25] plasmons, surface plasmon polaritons [26–28] are the examples. Electromagnetic field concentration allows more efficient optical heating [29, 30], enhancement of nonlinear [31] and magneto-optical [32–34] effects as well as the reduction of threshold pulse energy [35, 36] and detection sensitivity [37] in ultrafast laser demagnetization experiments. However, nanostructuring results in the appearance of additional ultrafast processes with new timescales. It was shown that such mechanisms as plasmon-induced interband transitions [38], electron diffusion under inhomogeneous heating [39], thermoacoustic [40, 41] and low-dimensional [42] effects appear in nanostructures and have to be taken into account. All these features can affect ultrafast magnetic dynamics in nanostructured ferromagnetic films.

In this paper, we experimentally show ultrafast 50% decrease in magneto-optical Kerr effect induced by femtosecond pump pulse in bulk nickel with subwavelength surface corrugation. The fluence is comparable to that required to achieve similar values in thin films. Numerical calculations show that the decrease does not correspond to uniform 50% reduction of entire surface magnetization but is the result of the appearance of demagnetized and non-demagnetized areas of surface.

The one-dimensional magnetoplasmonic crystal (MPC) is a 500-μm-thick nickel plate with wavy surface. The sample was fabricated by electron beam lithography and electroplating. First, a 500 nm layer of negative photoresist was deposited on a glass substrate that was then exposed by an electron beam to form a pattern. Then the resist was developed and a thin conductive layer of silver (~50 nm) was deposited on the mask. The 500-μm-thick nickel layer was grown on top of the latter by means of electroplating. The nickel was mechanically separated from the surface of photoresist. The silver layer was removed chemically.

The MPC was characterized by atomic force microscopy (AFM) and scanning electron microscopy (SEM). The sample surface shape is close to sinusoidal, the amplitude of the first spatial harmonic is 45 nm, that corresponds to the modulation depth of

90 nm, the amplitudes of the second and higher spatial harmonics do not exceed 2 nm. The grating period of the sample is 503 ± 2 nm. The sample has already been studied in detail by optical and magneto-optical means [32]. It supports the excitation of surface plasmon polaritons for a wide range of incidence angles in the visible spectral range. The spatial configuration of the sample surface provides the fulfillment of critical coupling condition ($\Gamma_{abs} = \Gamma_{rad}$) [30, 32]. A Fano-type resonance with close to zero minimal reflectance was observed. Resonant transverse magneto-optical Kerr effect (TMOKE) reached the value of 2.4×10^{-2} that corresponded to 77-fold enhancement in comparison with plane film. Ultrafast processes in the studied sample caused by laser heating with 800-nm pump pulse with 7 mJ/cm^2 fluence at the resonant probe wavelength of 645 nm were studied earlier [37]. A 6% reflectance change and 65% TMOKE reduction from 1.2×10^{-2} to 4×10^{-3} were observed.

Ultrafast laser demagnetization of nickel magneto-plasmonic crystal is studied here by the pump–probe technique. A regeneratively amplified Ti:sapphire laser (Coherent Libra) with 800-nm central wavelength, 70-fs pulse duration, and 1 kHz repetition rate was used as a source of laser radiation. The normally incident non-resonant 800-nm pump pulse heated the sample surface. The probe pulse was TM-polarized supercontinuum (500–1400 nm) generated in the sapphire plate. The angle of incidence to the sample was 12° that corresponded to 620-nm resonant wavelength. The supercontinuum spectrum above 750 nm were cut off by shortpass photonic crystal filter. The pump and probe fluences were 6 mJ/cm^2 and 1 nJ/cm^2, respectively. Spot diameters on the sample surface were 700 and 400 μm, respectively. The saturating magnetic field of 500 Oe was applied in transverse configuration.

The measured magneto-optical contrast $\Delta\delta$ was defined as absolute difference between TMOKE values in the presence and the absence of pump pulse:

$$\Delta\delta(\tau) = \delta_{\text{pump}}(\tau) - \delta_{\text{nopump}}, \quad (1)$$

where τ is pump–probe delay. The following equation was used to define δ value:

$$\delta = 2\frac{R(H) - R(-H)}{R(H) + R(-H)}. \quad (2)$$

Experimental magneto-optical contrast spectra of the studied MPC at various pump–probe delays are shown in top panel of Fig. 1. The most significant $\Delta\delta$ change is observed within the resonant spectral range from 600 to 640 nm. The TMOKE change reaches its maximum at $\tau = 500$ fs pump–probe delay that is close to the nickel demagnetization time [1]. Magneto-optical contrast $\Delta\delta$ spectrum for this pump–probe delay is shown in the bottom panel of Fig. 1 along with TMOKE spectra δ_{pump} (blue circles) and δ_{nopump} (blue line). Laser heating shifts the TMOKE resonance by 3 nm and halves its absolute values. The spectral changes can be governed by either laser-induced nickel demagnetization or modification of surface plasmon wave vector k_{SPP}. Change of its real part ($\Delta k'_{SPP} \neq 0$) should result in the plasmon resonance shift while the modification of its imaginary part ($\Delta k''_{SPP} \neq 0$) should affect the resonance Q-factor. Since no broadening of TMOKE spectrum is observed the modification of surface plasmon wave vector upon laser heating is limited to its real part. One can obtain the contribution of nickel demagnetization into the $\Delta\delta$ modulation by compensating the corresponding shift of plasmon resonance. The shift of δ_{nopump} line by 3 nm to longer wavelengths and the twofold reduction of its absolute values results in δ^*_{nopump} line (shown by violet dashed line in bottom panel in Fig. 1). The latter almost coincides with the δ_{pump} line. Thus, the laser-induced demagnetization of nickel MPC by 70-fs 800-nm laser pulse with energy density of 6 mJ/cm^2 causes 50% reduction of TMOKE absolute values within the spectral range of plasmon resonance.

The observed decrease in TMOKE values in the bulk MPC at the given pump pulse energy density is typical to thin nickel films with a thickness of 15–20 nm [1, 11, 43]. However, it is known that bulk samples are demagnetized weaker than films [44]. It was shown that 65% demagnetization of bulk nickel requires fluences comparable with the nickel melting threshold [45]. The inconsistency can be attributed to the sample surface curvature. It affects both temperature and probe near-field distributions.

Steady-state distribution of near-field in studied sample as well as the distributions of absorbed energy at the pump (800 nm) and probe (617 nm) wavelengths were calculated in Comsol Multiphysics. Sample configuration (corrugation depth, spatial period) as well as experimental conditions (angles of incidence of both beams, polarization, pump fluence) were reproduced in the model. The temperature calculation was carried out within the two-temperature model [46] that is the system of two parabolic partial differential equation describing the heat coupling of electrons and phonons in metals:

$$\begin{cases} \gamma T_e \dfrac{\partial T_e}{\partial t} = \nabla(K_e \nabla T_e) - g(T_e - T_l) + S(r,t) \\ C_l \dfrac{\partial T_l}{\partial t} = \nabla(K_l \nabla T_l) + g(T_e - T_l). \end{cases} \quad (3)$$

Here, γT_e and C_l are electron and lattice heat capacities, K_e and K_l are thermal conductivities of an electron gas and lattice, respectively, g is a coupling constant that characterizes the energy transfer from hot electrons to the lattice, $S(r,t)$ is a source term. The

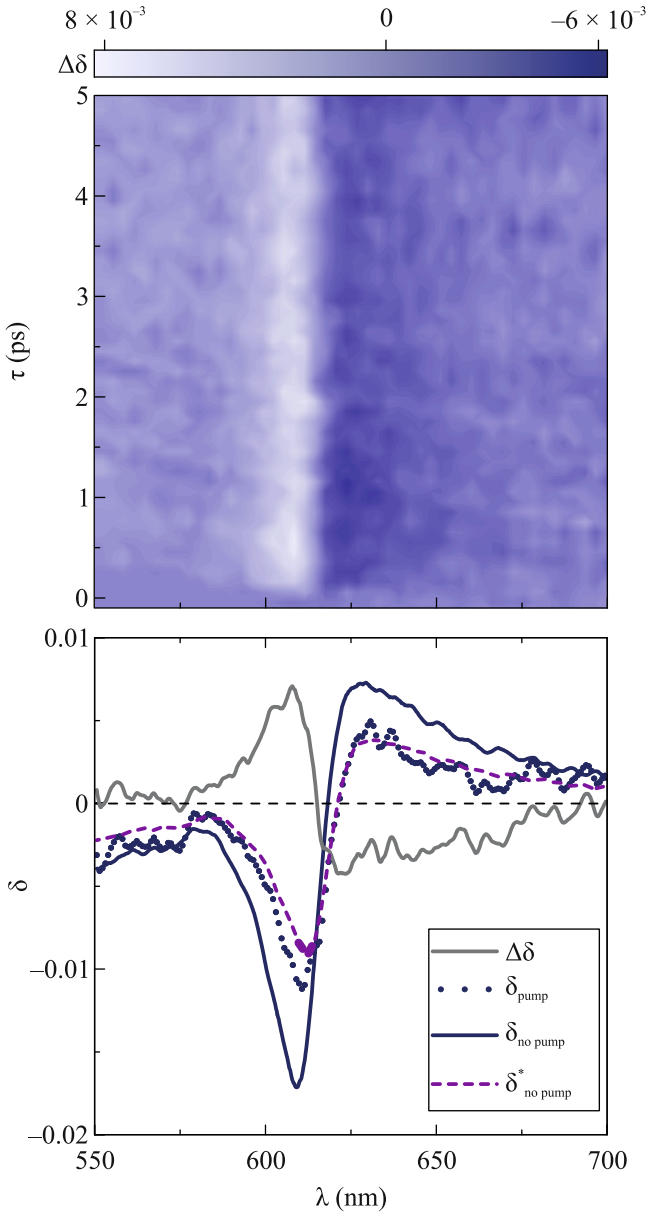

Fig. 1. (Color online) Top panel: magneto-optical contrast $\Delta\delta$ versus the pump–probe delay τ and probe wavelength λ. Bottom panel: magneto-optical contrast spectra (gray line) taken at 500-fs pump–probe delay. TMOKE spectra in the presence (δ_{pump}, blue circles) and the absence ($\delta_{no\,pump}$, blue line) of the pump pulse. The description of the violet dashed line is given in the text.

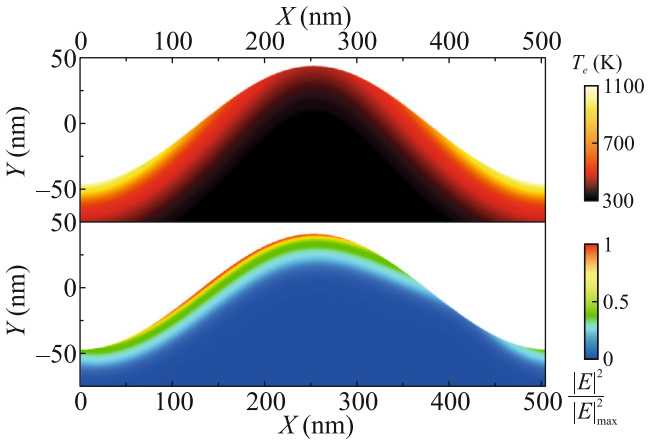

Fig. 2. (Color online) Top panel: the electron temperature distribution within a single spatial period of studied sample at $\tau = 500$ fs. Bottom panel: the normalized distribution of the squared electric near-field of the probe pulse in the sample at the wavelength of plasmon excitation (617 nm).

$S(r,t)$ spatial profile corresponds to the distribution of calculated absorbed energy at pump wavelength, while the temporal dependence follows the envelope of the pump pulse. The system of differential Eqs. (3) allows one to find spatial distributions of the electron T_e and lattice T_l temperature at various pump–probe delays. The values of γ, K_e, g, C_l, K_l were chosen to fit well the temporal dependency of differential reflectivity to the experimental data obtained earlier [37].

The calculated distribution of electron gas temperature at the delay of $\tau = 500$ fs that corresponds to maximal T_e is shown in the top panel of Fig. 2. Nonuniform heating of studied MPC surface is observed: the heat is concentrated mainly in the grating grooves while the hills remain cold. The temperature in the heated areas is higher than that in the plane films at the same pump fluence level [1], while the temperature in cold areas is lower. Since the demagnetization follows the temperature dynamics, the sample magnetization distribution is strongly inhomogeneous in contrast to a plane film. Thus, the spatial distribution of probe pulse near-filed defined by the surface plasmon localization (bottom panel in Fig. 2) starts to play a crucial role. The probed area overlaps only partially with the hottest regions. It results in 50% magneto-optical Kerr effect decrease that is comparable to that in thin films under similar fluence values [1, 11, 43].

In conclusion, ultrafast 50% decrease in transverse magneto-optical Kerr effect within the spectral range of plasmon excitation is observed in all-nickel magnetoplasmonic crystal under 6 mJ/cm^2 femtosecond pump. The value for the bulk samples were expected to be at several times higher fluences [8, 45]. Numerical calculations of probe pulse near-field and MPC temperature distributions were carried out to explain the observed feature. TMOKE reduction is not attributed to the uniform decrease in the entire surface magnetization but to its inhomogeneous heating. The grating grooves are heated more intensively than the plane films under similar conditions. As a result only a part of the sample surface becomes demagnetized. Thus, macroscopic ultrafast magneto-optical response relates to the magnetization state indirectly in more

complex way in nanostructure systems. It requires an additional consideration and interpretation in each particular case.

FUNDING

This work was supported by the Russian Foundation for Basic Research (project no. 22-22-00856). I.A. Novikov and M.A. Kiryanov acknowledge the support of the Foundation for the Advancement of Theoretical Physics and Mathematics BASIS.

CONFLICT OF INTEREST

The authors of this work declare that they have no conflicts of interest.

REFERENCES

1. E. Beaurepaire, J.-C. Merle, A. Daunois, and J.-Y. Bigot, Phys. Rev. Lett. **76**, 4250 (1996).
2. M. Pankratova, I. P. Miranda, D. Thonig, M. Pereiro, E. Sjöqvist, A. Delin, O. Eriksson, and A. Bergman, Phys. Rev. B **106**, 174407 (2022).
3. B. Mueller and B. Rethfeld, Phys. Rev. B **90**, 144420 (2014).
4. B. Koopmans, J. J. M. Ruigrok, F. Dalla Longa, and W. J. M. de Jonge, Phys. Rev. Lett. **95**, 267207 (2005).
5. K. Carva, M. Battiato, and P. M. Oppeneer, Phys. Rev. Lett. **107**, 207201 (2011).
6. Z. Zheng, Q. Zheng, and J. Zhao, Phys. Rev. B **105**, 085142 (2022).
7. U. Atxitia and O. Chubykalo-Fesenko, Phys. Rev. B **84**, 144414 (2011).
8. K. Krieger, J. Dewhurst, P. Elliott, S. Sharma, and E. Gross, J. Chem. Theory Comput. **11**, 4870 (2015).
9. S. R. Acharya, V. Turkowski, G. Zhang, and T. S. Rahman, Phys. Rev. Lett. **125**, 017202 (2020).
10. H. Hamamera, F. S. M. Guimarães, M. dos Santos Dias, and S. Lounis, Commun. Phys. **5**, 16 (2022).
11. A. Eschenlohr, M. Battiato, P. Maldonado, N. Pontius, T. Kachel, K. Holldack, R. Mitzner, A. Föhlisch, P. M. Oppeneer, and C. Stamm, Nat. Mater. **12**, 332 (2013).
12. G. Salvatella, R. Gort, K. Bühlmann, S. Däster, A. Vaterlaus, and Y. Acremann, Struct. Dyn. **3**, 055101 (2016).
13. K. Krieger, P. Elliott, T. Müller, N. Singh, J. Dewhurst, E. Gross, and S. Sharma, J. Phys.: Condens. Matter **29**, 224001 (2017).
14. K. Kuiper, G. Malinowski, F. Dalla Longa, and B. Koopmans, J. Appl. Phys. **109**, 07D316 (2011).
15. Y. Kivshar, Nano Lett. **22**, 3513 (2022).
16. A. A. Popkova, I. M. Antropov, G. I. Tselikov, G. A. Ermolaev, I. Ozerov, R. V. Kirtaev, S. M. Novikov, A. B. Evlyukhin, A. V. Arsenin, V. O. Bessonov, V. S. Volkov, and A. A. Fedyanin, Laser Photon. Rev. **16**, 2100604 (2022).
17. Z. Sadrieva, K. Frizyuk, M. Petrov, Y. Kivshar, and A. Bogdanov, Phys. Rev. B **100**, 115303 (2019).
18. A. M. Chernyak, M. G. Barsukova, A. S. Shorokhov, A. I. Musorin, and A. A. Fedyanin, JETP Lett. **111**, 46 (2020).
19. D. O. Ignatyeva, D. Karki, A. A. Voronov, M. A. Kozhaev, D. M. Krichevsky, A. I. Chernov, M. Levy, and V. I. Belotelov, Nat. Commun. **11**, 5487 (2020).
20. D. A. Shilkin and A. A. Fedyanin, JETP Lett. **115**, 136 (2022).
21. B. I. Afinogenov, V. O. Bessonov, I. V. Soboleva, and A. A. Fedyanin, ACS Photon. **6**, 844 (2019).
22. K. A. Willets and R. P. van Duyne, Ann. Rev. Phys. Chem. **58**, 267 (2007).
23. N. Maccaferri, A. Gabbani, F. Pineider, T. Kaihara, T. Tapani, and P. Vavassori, Appl. Phys. Lett. **122**, 120502 (2023).
24. V. G. Kravets, A. V. Kabashin, W. L. Barnes, and A. N. Grigorenko, Chem. Rev. **118**, 5912 (2018).
25. A. I. Musorin, A. V. Chetvertukhin, T. V. Dolgova, H. Uchida, M. Inoue, B. S. Luk'yanchuk, and A. A. Fedyanin, Appl. Phys. Lett. **115**, 151102 (2019).
26. W. L. Barnes, A. Dereux, and T. W. Ebbesen, Nature (London, U.K.) **424**, 824 (2003).
27. M. R. Shcherbakov, P. P. Vabishchevich, A. Yu. Frolov, T. V. Dolgova, and A. A. Fedyanin, Phys. Rev. B **90**, 201405 (2014).
28. D. V. Murzin, A. Yu. Frolov, K. A. Mamian, V. K. Belyaev, A. A. Fedyanin, and V. V. Rodionova, Opt. Mater. Express **13**, 171 (2023).
29. A. N. Koya, M. Romanelli, J. Kuttruff, et al., Appl. Phys. Rev. **10**, 021318 (2023).
30. D. Ryabov, O. Pashina, G. Zograf, S. Makarov, and M. Petrov, Nanophotonics **11**, 3981 (2022).
31. G. Zograf, K. Koshelev, A. Zalogina, V. Korolev, R. Hollinger, D.-Y. Choi, M. Zuerch, C. Spielmann, B. Luther-Davies, D. Kartashov, S. V. Makarov, S. S. Kruk, and Y. Kivshar, ACS Photon. **9**, 567 (2022).
32. M. A. Kiryanov, A. Yu. Frolov, I. A. Novikov, P. A. Kipp, P. K. Nurgalieva, V. V. Popov, A. A. Ezhov, T. V. Dolgova, and A. A. Fedyanin, APL Photon. **7**, 026104 (2022).
33. V. K. Belyaev, V. V. Rodionova, A. A. Grunin, M. Inoue, and A. A. Fedyanin, Sci. Rep. **10**, 7133 (2020).
34. A. Yu. Frolov, M. R. Shcherbakov, and A. A. Fedyanin, Phys. Rev. B **101**, 045409 (2020).
35. M. Kataja, F. Freire Fernandez, J. Witteveen, T. Hakala, P. Törmä, and S. Dijken, Appl. Phys. Lett. **112**, 072406 (2017).
36. H. Xu, G. Hajisalem, G. Steeves, R. Gordon, and B.-C. Choi, Sci. Rep. **5**, 15933 (2015).
37. I. A. Novikov, M. A. Kiryanov, P. K. Nurgalieva, A. Yu. Frolov, V. V. Popov, T. V. Dolgova, and A. A. Fedyanin, Nano Lett. **20**, 8615 (2020).
38. M. Taghinejad, H. Taghinejad, Z. Xu, K.-T. Lee, S. P. Rodrigues, J. Yan, A. Adibi, T. Lian, and W. Cai, Nano Lett. **18**, 5544 (2018).

39. A. Schirato, M. Maiuri, A. Toma, S. Fugattini, R. Proietti Zaccaria, P. Laporta, P. Nordlander, G. Cerullo, A. Alabastri, and G. della Valle, Nat. Photon. **14**, 723 (2020).
40. G. V. Hartland, Chem. Rev. **111**, 3858 (2011).
41. M. A. Kiryanov, G. S. Ostanin, T. V. Dolgova, M. Inoue, and A. A. Fedyanin, JETP Lett. **117**, 196 (2023).
42. C. Voisin, D. Christofilos, N. Del Fatti, F. Vallée, B. Prével, E. Cottancin, J. Lermé, M. Pellarin, and M. Broyer, Phys. Rev. Lett. **85**, 2200 (2000).
43. T. Roth, A. J. Schellekens, S. Alebrand, O. Schmitt, D. Steil, B. Koopmans, M. Cinchetti, and M. Aeschlimann, Phys. Rev. X **2**, 021006 (2012).
44. K. Krieger, P. Elliott, T. Müller, N. Singh, J. Dewhurst, E. Gross, and S. Sharma, J. Phys.: Condens. Matter **29**, 224001 (2017).
45. U. Bierbrauer, S. T. Weber, D. Schummer, M. Barkowski, A.-K. Mahro, S. Mathias, H. C. Schneider, B. Stadtmüller, M. Aeschlimann, and B. Rethfeld, J. Phys.: Condens. Matter **29**, 244002 (2017).
46. S. I. Anisimov, B. L. Kapeliovich, and T. L. Perel'man, J. Exp. Theor. Phys. **39**, 375 (1974).